



# A novel cold air electrostatic minimum quantity lubrication (CAEMQL) technique for the machining of titanium alloys Ti–6Al–4 V

Fucui Liu<sup>1,2</sup> · Xizhuan Wu<sup>1,2</sup> · Yu Xia<sup>1,2</sup> · Tao Lv<sup>3</sup> · Ruochong Zhang<sup>1,2</sup> · Xiaodong Hu<sup>1,2</sup> · Xuefeng Xu<sup>1,2</sup>

Received: 9 August 2022 / Accepted: 4 March 2023 / Published online: 1 April 2023  
© The Author(s), under exclusive licence to Springer-Verlag London Ltd., part of Springer Nature 2023

## Abstract

The milling of titanium alloys is usually associated with a high cutting temperature and severe tool wear. Therefore, flood cooling technologies have been conventionally employed to prolong the tool life and improve the quality of the machined surface. However, the negative impact on the environment and waste disposal problems caused by the vast quantity of metalworking fluids used in the process have become significant. In this study, a new machining method called “cold air electrostatic minimum quantity lubrication (CAEMQL)” is proposed for machining titanium alloy Ti–6Al–4 V. The milling performance of CAEMQL was systematically assessed in terms of cutting force, cutting temperature, surface roughness, tool life, tool wear, and chip morphology, using minimum quantity lubrication (MQL), electrostatic minimum quantity lubrication (EMQL), and cold air minimum quantity lubrication (CAMQL) as benchmarks. It was found that CAEMQL resulted in improved critical heat flux and steady-state heat transfer performance compared to MQL, EMQL, and CAMQL, which thus produced a lower milling force, smaller milling temperature, better surface quality, and less tool wear. The degree of chip segmentation was enhanced with less deformation under CAEMQL due to its synergistic cooling and lubrication effect.

**Keywords** Cold air electrostatic minimum quantity lubrication · Titanium alloy · Heat transfer characteristics · Milling performance · Chip morphology

## 1 Introduction

Titanium alloys are widely used in aerospace, medical, and military fields because of their high strength-to-weight ratio, fracture toughness, high-temperature stability, and good anti-corrosion properties [1–3]. However, their low thermal conductivity, high chemical activity, and small elastic modulus render them difficult-to-cut materials as high cutting temperatures and severe tool wear are easily induced during machining [4, 5]. Conventionally, flood cooling technologies are primarily employed during milling processes. However,

the usage of cutting fluids frequently causes major environmental problems and employee health concerns because it contains a large number of harmful substances and greatly increases the total production cost, which means that the current requirement of green, efficient, sustainable development is not being met [6–8]. All the above points have motivated researchers to search for alternatives to minimize cutting fluid usage and improve the machining performance of titanium alloys. Some alternatives have been proposed, such as dry cutting [9], minimum quantity lubrication (MQL) [10], electrostatic minimum quantity lubrication (EMQL) [11], cryogenic minimum quantity lubrication (CMQL) [12], and cold air with minimum quantity lubrication (CAMQL) [13].

Dry cutting is a kind of green, low-processing-cost, and environmentally friendly cutting method that has been applied in the processing of gray cast iron, pure aluminum, and magnesium alloy. However, dry cutting cannot satisfy the process conditions of titanium alloy milling due to its serious lack of cooling and lubrication performance [14, 15].

As a new type of lubrication and cooling method, the MQL technique has been widely used in turning, milling, drilling, and grinding due to its favorable lubrication, low

✉ Xuefeng Xu  
xuxuefeng@zjut.edu.cn

<sup>1</sup> College of Mechanical Engineering, Zhejiang University of Technology, Hangzhou 310023, China

<sup>2</sup> Key Laboratory of Special Purpose Equipment and Advanced Processing Technology, Ministry of Education and Zhejiang Province, Zhejiang University of Technology, Hangzhou 310023, China

<sup>3</sup> Department of Mechanical Engineering, Ningbo Polytechnic, 288Lushan Road, Ningbo 315800, China

processing cost, and low pollution [16–18]. With the MQL method, the amount of cutting fluid used during machining is reduced [19]. A very small amount of lubricant is delivered to the cutting region in the form of small droplets [20–22], which reduce the cutting force and temperature and improve machining quality [23–26]. For example, Dhar et al. [27] used the MQL technique in the turning processes of medium-carbon steel. They concluded that MQL had improved machining performance compared to wet cutting in some cases. Tasdelen et al. [28] investigated the effects of MQL, wet cutting, and air cooling on surface roughness, tool wear, and cutting force when drilling hardened steel. They reported that MQL outperformed air cooling and wet cutting in terms of tool wear. Krishnan et al. [29] conducted a drilling experiment of AISI 304 with MQL. They found that MQL had a machining performance often exceeding that of flood lubrication with respect to the life, cutting force, and drilled hole diameter error. Sun et al. [30] studied the effects of dry cutting, MQL, and MQL-mixed water on the milling force, tool life, cutting temperature, surface roughness, and topography when milling GH4099 using ceramic tools. They found that MQL outperformed dry cutting in terms of cutting temperature, milling force, tool life, and surface roughness. Shen et al. [31] studied the wear and friction characteristics of grinding when grinding cast iron under wet, dry cutting, and MQL. Their investigation suggested that MQL remarkably reduced the grinding temperature compared to dry cutting. However, the titanium alloy chip and workpiece maintain very close contact with the tool on the rake face and flank face due to the high cutting temperature and load. Therefore, oil mists cannot effectively penetrate the contact layer to lubricate the cutting zone under MQL [32–34].

To solve the issue of MQL heat transfer, some researchers proposed the CMQL technique, which uses liquid nitrogen ( $\text{LN}_2$ ) and liquid  $\text{CO}_2$  ( $\text{LCO}_2$ ) as cooling media with MQL to cool and lubricate the cutting area. Cetindag et al. [35] reported that MQL- $\text{CO}_2$  significantly reduced the tool wear of both conventional and wiper inserts. Gross et al. [36] compared the variable energy consumption when milling

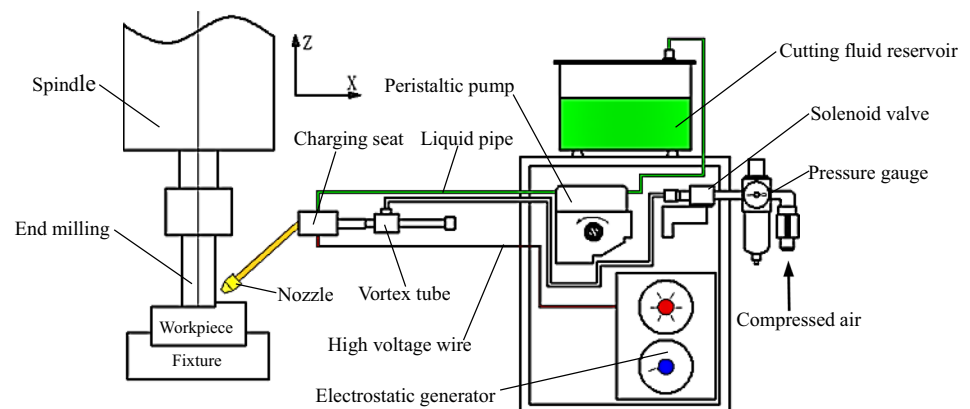
Ti-6Al-4 V with  $\text{CO}_2$ -based CMQL and wet cutting. Their investigation suggested that CMQL made a decisive contribution to reducing the energy demand. Sanchez et al. [37] carried out grinding experiments using MQL- $\text{CO}_2$ . Their results showed that the frozen oil layer protected the integrity of abrasive grains, significantly improved the life of the grinding wheel, and reduced thermal damage to the workpiece. Hong and Ding [38] studied a turning experiment of titanium alloy Ti-6Al-4 V under cryogenic, dry cutting, and wet cutting. They found that a small amount of liquid nitrogen applied locally to the cutting edge was superior to wet cutting in terms of cutting temperature. However, the cost of  $\text{LN}_2$  was high, and the low-temperature effect under MQL- $\text{LN}_2$  led to the work hardening of titanium alloy, eventually causing an increase in the cutting force and tool wear [39–41].

In addition, some researchers proposed the CAMQL technique because the cooling mediums of MQL- $\text{CO}_2$  and MQL- $\text{LN}_2$  are expensive. Shokrani et al. [42] examined the influence of CAMQL on wear profiles and surface quality. Since the wear rate and surface quality are closely correlated with the cutting zone temperature, they found that CAMQL had 39% less surface roughness compared to dry machining of titanium alloy. Yuan et al. [32] used CAMQL in the milling processes of the titanium alloy Ti-6Al-4 V. They concluded that CAMQL resulted in a lower cutting force, tool wear, and surface roughness and produced shorter chips than dry cutting, wet cutting, and MQL. Moreover, CAMQL increased heat transfer, reduced cutting temperature, and maintained

**Table 1** Air pressure and temperature of vortex tube

Inlet pressure (MPa)	Inlet air jet temperature ( $^{\circ}\text{C}$ )	Outlet pressure of the cold end (MPa)	Outlet temperature of the cold end ( $^{\circ}\text{C}$ )
0.6	20	0.2	-5
		0.3	-1
		0.4	4

**Fig. 1** Schematic diagram of the CAEMQL system



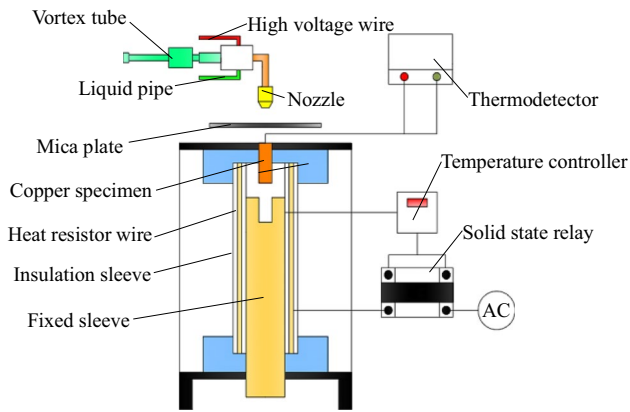


**Fig. 2** Schematic diagram of the transient heat exchange test device

the strength of an oil film to obtain better lubrication [43]. Zhang et al. [44] found that the cutting fluids of CAMQL quickly penetrated into tool-chip and tool-workpiece interfaces to form a lubricating film in the gear hobbing process, which inhibited the generation of friction heat. Saberi et al. [13] used CAMQL in the grinding processes of CK45 soft steel. They found that CAMQL significantly reduced the tangential grinding force and the friction coefficient compared to dry and wet cutting. Mitrofanov [45] and Krutikova [46] et al. used CAMQL in the grinding process and concluded that CAMQL reduced the temperature in the cutting area and decreased the power load.

Moreover, EMQL, as a technique using the synergetic effects of electrostatic spraying (ES) and minimum quantity lubrication (MQL), generates charged mist to spray the machining area for cooling and lubricating the tool-chip contact interfaces. Acceptable results were reported for the application of EMQL in turning, milling, and grinding. Xu et al. [11] used EMQL in the end-milling process of AISI-304 stainless steel. They found that EMQL achieved a lower cutting force, tool wear, surface roughness, and a higher tool life compared to dry cutting, wet cutting, and MQL. Lin et al. [47] used the EMQL technique in the grinding process of 45 medium-carbon steel. They concluded that charged lubricant droplets easily entered and covered the wheel-workpiece interfaces, which improved the capacity of lubrication and heat transfer on the grinding areas compared to conventional MQL. Huang et al. [48] found that EMQL considerably enhanced tribological performance and reduced lubricant consumption compared to MQL. Huang et al. [49] used EMQL in the turning process of stainless steels. They found that properly selecting cutting parameters was achieved by promoting lubricants into the cutting interface to reduce friction and adhesion of workpiece materials on the interface. Wang et al. [16] found that EMQL can realize the effective lubrication of the friction interface in the turning process through the spraying of the atomized

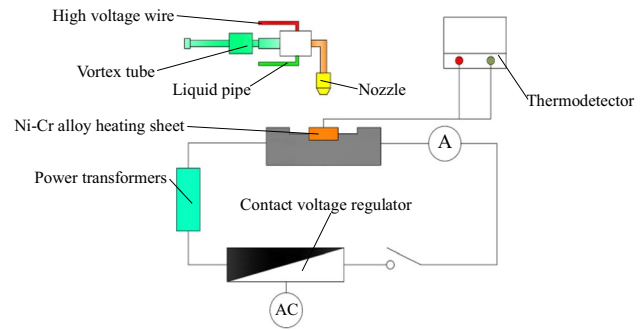


**Fig. 3** Schematic diagram of the steady-state heat transfer test device

lubricating medium. Lv et al. [50] found that the EMQL technique when milling 304 stainless steel increased capillary penetration force and penetration depth of water-based nanofluid cutting fluid by 34% and 16%, respectively. The results showed that EMQL considerably improved the permeability and anti-wear and anti-friction properties of the lubricant. Bartolomeis et al. [51] reported that EMQL performed better than MQL in terms of surface integrity when high-speed milling Inconel 718.

Considering the required conditions, cold air electrostatic minimum quantity lubrication (CAEMQL) is designed and developed in this paper. By combining the cooling performance of CAMQL and the lubricating performance of EMQL, the feasibility of milling the titanium alloy Ti-6Al-4 V using this new technology is investigated by analyzing the heat transfer characteristics and milling performance.

The aim of this study is to compare the effectiveness of CAEMQL with that of MQL, EMQL, and CAMQL machining when end-milling the titanium alloy Ti-6Al-4 V at industrial speed feed combinations using coated cemented carbide mills. The tool life, cutting forces, cutting

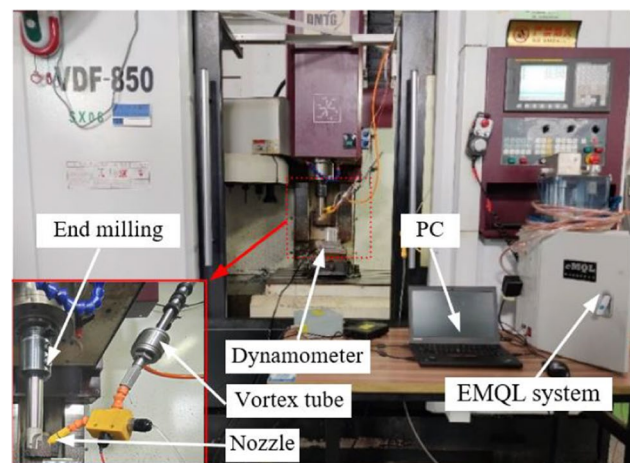


**Fig. 4** Photographic view of the experimental set-up

temperature, surface roughness, and chip morphology that result from applying CAEMQL in end milling are comparatively investigated.

## 2 Experimental details

### 2.1 CAEMQL system

Figure 1 shows the CAEMQL end-milling system. The cutting fluids were continuously pumped from the cutting fluid reservoir to the liquid pipe using a peristaltic pump, and the fluid flow was controlled within 20–200 mL/h. The high-voltage negative electricity from the electrostatic generator was embedded in the liquid pipe to make full contact with the cutting fluid in a charging seat so that the cutting fluids were charged. The cold compressed air was provided by an AH20025

vortex tube (American AiRTX Co.) and entered into the charging seat. Subsequently, the charged cutting fluid and cold-compressed air were mixed in the nozzle, and then the charged oil mist was formed and transported from the nozzle to the cutting area. It was assumed that  $-6$  kV would be effective in obtaining fine-charged oil mists [48]. The nozzle was kept at a 20-mm distance from the machining area. As shown in Table 1, the air pressure and temperature of the vortex tube were measured. To ensure a better cooling effect, the outlet air pressure and the jet temperature of the cold end were 0.2 MPa and  $-5$  °C, respectively. The cutting fluid was a water-based cutting fluid, type QC-3801 (Tsinghua Tianjin Research Institute for Advanced Equipment, China), which was beneficial for improving the atomization characteristics of the droplets and forming a chemical adsorption film easily to play anti-friction and anti-wear roles [52].

**Table 2** Chemical composition of TC4 titanium alloy (wt.%)

Ti	Al	V	Fe	O	C	N	H
Balanced	6.15	4.40	0.09	0.08	0.05	0.01	0.005

**Table 3** Physical and mechanical properties of TC4 titanium alloy

Parameter	Value	Parameter	Value
Density $\rho_0$ (kg/m <sup>3</sup> )	4430	Yield strength $\sigma_s$ (MPa)	820
Melting temperature (°C)	1668	Elasticity modulus $E$ (GPa)	113.8
Thermal conductivity $K$ (W/(m·K))	7.3	Poisson's ratio $\mu$	0.342
Tensile strength $\sigma_b$ (MPa)	950	Specific heat $c$ (J/(kg·°C))	526
Expansion rate $\alpha$ (%)	14.0		

**Table 4** Milling conditions

Machine tool	VDF-850 vertical milling center, China
Workpiece material	TC4 titanium alloy Dimensions: 96 mm × 75 mm × 70 mm block
Inserts	APMT1604PDER-H08, Sumitomo Coated cemented carbide
Cutting parameters	Cutting speed: 120 m/min Feed rate: 0.1 mm/tooth Axial depth of the cut: 1 mm Radial depth of the cut: 5 mm
Wet conditions	QC-3801 water-based cutting fluid, Tsinghua University, China
Spraying mist parameters	Cutting fluid flow rate: 30 mL/h Cold-compressed air pressure: 0.2 MPa Nozzle distance: 20 mm
Environment	MQL with 20°C compressed air temperature CAMQL with $-5$ °C compressed air temperature EMQL with $-6$ kV charging voltage and 20°C compressed air temperature CAEMQL with $-6$ kV charging voltage and $-5$ °C compressed air temperature

## 2.2 Heat transfer test

### 2.2.1 Transient heat transfer test

The transient heat transfer test device is shown in Fig. 2, which reveals the transient heat transfer characteristics under CAEMQL. First, the electric furnace power supply was started, and the collected temperature from the K thermocouple was fed back to the ST507 intelligent temperature controller (Wenzhou Shangtong Instrument Ltd., China). The control signals were then output to the solid-state relay to control the on–off of the electric furnace power supply to realize constant temperature control of the furnace. Second, when the furnace was heated to a specified temperature, the insulation sleeve was raised to induce the adiabatic state surface of the copper specimen except for the upper surface.

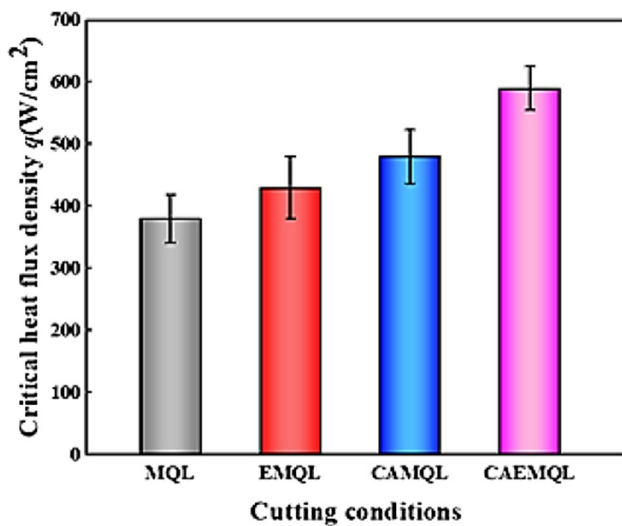
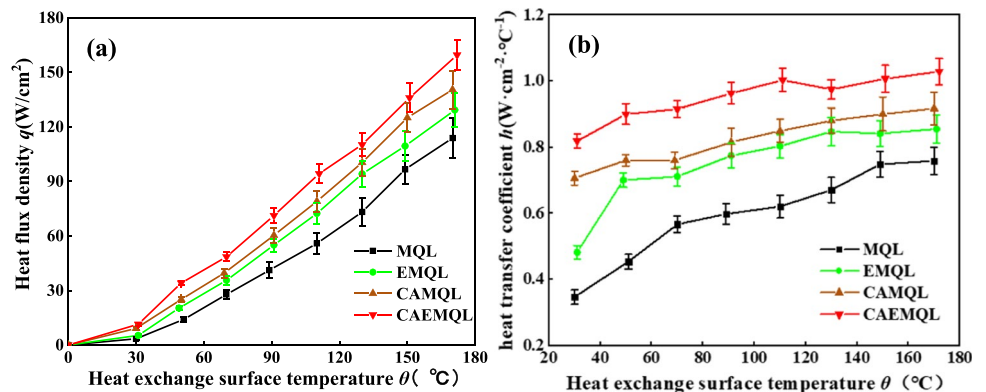


**Fig. 5** Critical heat flux at 170°C under different lubrication conditions (cutting fluid flow rate: 30 mL/h; nozzle distance: 20 mm; cold compressed air pressure: 0.2 MPa; charging voltage: –6 kV; cold compressed air temperature: –5°C)

**Fig. 6** Steady-state heat transfer performance of aerosol under different lubrication conditions: **a** heat flux density and **b** steady-state heat transfer coefficient (cutting fluid flow rate: 30 mL/h; nozzle distance: 20 mm; cold compressed air pressure: 0.2 MPa; charging voltage: –6 kV; cold compressed air temperature: –5°C)



Third, the CAEMQL system was started, and various parameters (charging voltage, air pressure, cutting fluid flow rate, nozzle distance) were adjusted. To achieve the uniform diffusion of charged mists, the nozzle was located directly above the copper. The mica plate was then quickly drawn out after the spray was stable. Low-temperature charged mists were directly sprayed on the upper surface of the copper, and the real-time temperature of the thermocouple was collected by an RX4006D thermodetector (Hangzhou Control Automation Technology Ltd., China), which allowed the temperature change curve of the heat exchange surface to be obtained. The critical heat flux of the heat transfer surface was obtained by a numerical analysis of one-dimensional heat conduction.

### 2.2.2 Steady-state heat transfer test

The cooling performance of four different lubrication conditions was measured under steady-state conditions using a steady-state heat transfer testing device, as shown in Fig. 3. A Ni–Cr alloy heating sheet with dimensions of 10 mm × 3 mm × 0.2 mm was continuously heated using a low-voltage and high alternating current to simulate a milling heat source. First, a k-type thermocouple connected with an RX4006D thermodetector was welded onto the surface of the heating sheet to monitor its surface temperatures online. Second, the CAEMQL device was turned on to cool the heating sheet. As the sheet temperature reached a constant value, the voltage and current of the sheet were recorded. Subsequently, the numerical calculation formulas of the surface heat flux density and heat transfer coefficient were employed as follows:

$$q = UI/A \tag{1}$$

$$h = q/(T_w - T_f) \tag{2}$$

where  $q$  is the surface heat flux density (W/cm<sup>3</sup>),  $U$  is the voltage value of the heating sheet (V),  $I$  is the current value

of the heating sheet ( $A$ ),  $A$  is the heat transfer area ( $0.3 \text{ cm}^2$ ),  $h$  is the heat transfer coefficient ( $\text{W}/\text{cm}^2/^\circ\text{C}$ ),  $T_w$  is the surface temperature of the specimen ( $^\circ\text{C}$ ), and  $T_f$  is the temperature of the lubricant droplets ( $^\circ\text{C}$ ).

### 2.3 Milling machining test

The machining tests were conducted with a DMTG VDF-850 vertical machining center. The CAEMQL system consisted of an EMQL system and a vortex tube. The experimental setup is shown in Fig. 4. Titanium alloy Ti-6Al-4 V with dimensions of  $96 \text{ mm} \times 75 \text{ mm} \times 70 \text{ mm}$  was selected as the cutting material, and the chemical composition and physical and mechanical properties are shown in Tables 2 and 3. Before the experiment, the surface of the workpiece was cut 1 mm thick to ensure consistent experimental

parameters. A cemented carbide insert coated with W (Sumitomo, Rineck, APMT1604PDER-H08) was employed as a cutting tool. A 35-mm-diameter milling cutter was used during the machining process. To ensure the same test conditions, each experiment was replaced with a new insert before testing. Table 4 presents the cutting experimental parameters.

The cutting forces under different lubrication conditions were measured with an FC3D120 three-dimensional dynamometer (Forcechina Measurement Technology Co.), and the experimental data of cutting forces  $F_x$ ,  $F_y$ , and  $F_z$  were recorded. The equation,  $F_r = (F_x^2 + F_y^2 + F_z^2)^{1/2}$ , was used to calculate the resultant force ( $F_r$ ). The temperature of the cutting area in the milling process was collected by a hand-held online thermal imager (FOTRIC 226, Germany), which is an indirect measurement method. Although the real temperature of the tool could not be

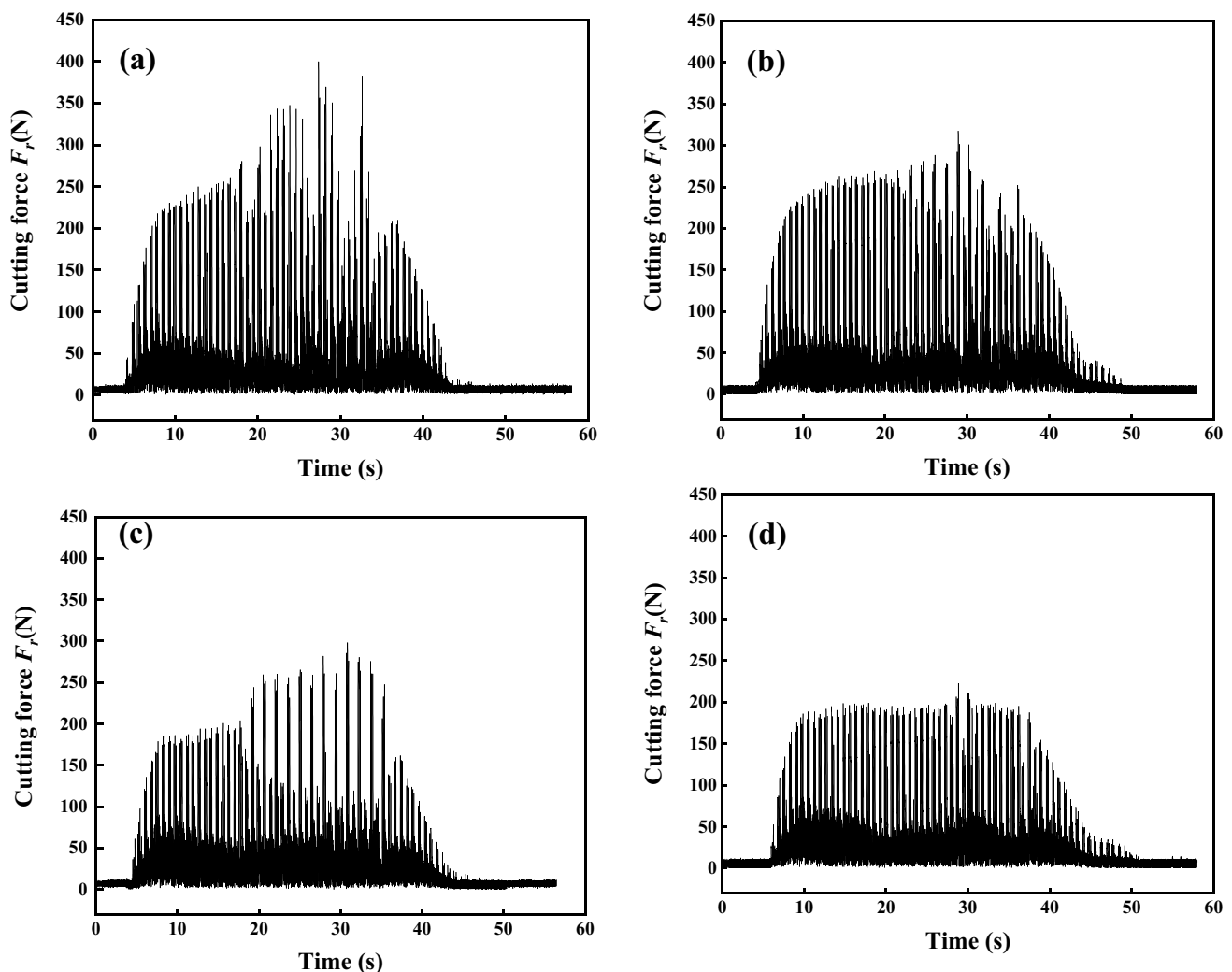


**Fig. 7** Cutting force signal diagram under different lubrication conditions: **a** MQL, **b** EMQL, **c** CAMQL, and **d** CAEMQL (cutting speed: 120 m/min; axial depth of cut: 1 mm; radial depth of cut: 5 mm; feed rate: 0.1 mm/tooth)

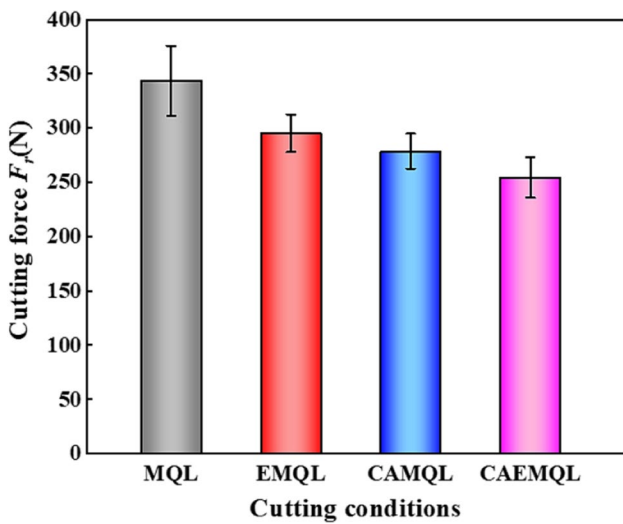


**Fig. 8** Average cutting force under different lubrication conditions (cutting speed: 120 m/min; axial depth of cut: 1 mm; radial depth of cut: 5 mm; feed rate: 0.1 mm/tooth)

obtained, the indirectly measured temperature of the tool could be used to compare cutting temperatures under different lubrication conditions. The surface roughness of the workpiece  $R_a$  (arithmetic mean roughness) was measured at ten specific points along the cutting direction (i.e., along the 96-mm direction) using a portable surface roughness tester (SJ-210, Mitutoyo, Japan) with a sampling length of 0.8 mm. An optical microscope (VW-6000, Keyence,

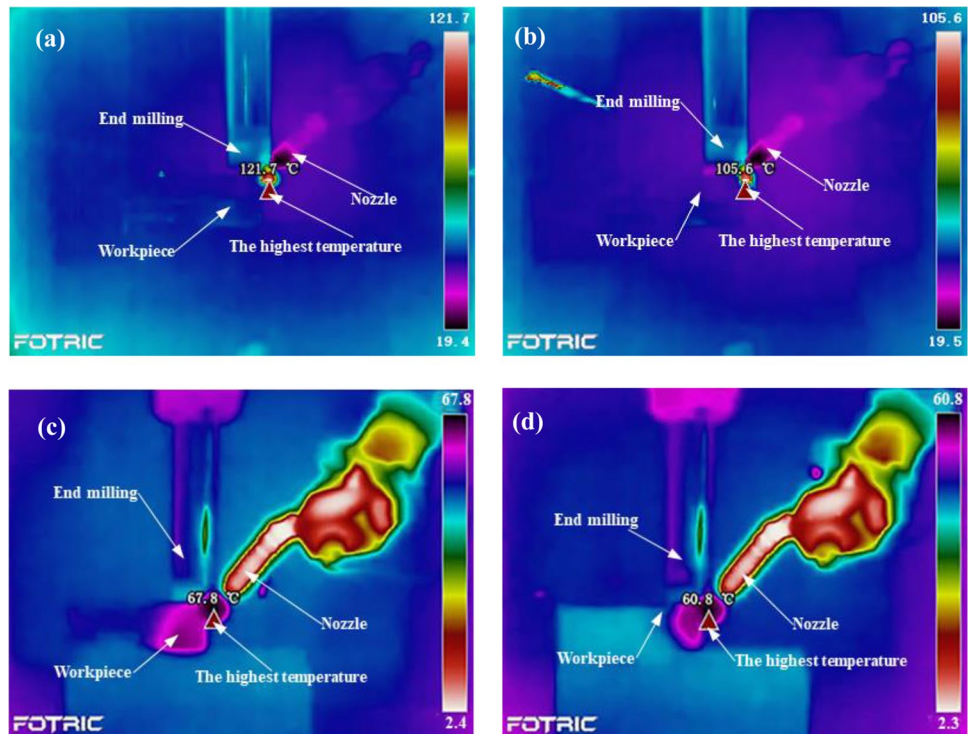
Japan) was used to measure the flank wear of the tools under different lubrication conditions, and the wear morphology was comparatively analyzed. The tool life was defined as the machining time at which the maximum flank wear reached 0.3 mm. The worn tool was examined with a scanning electron microscope (EVO18, Zeiss, Germany) to analyze the predominant type of wear mechanisms. A VW-6000 optical microscope was used to observe the free surface and back surface of titanium alloy Ti-6Al-4 V chips under different lubrication conditions.

### 3 Results and discussion

#### 3.1 Heat transfer characteristics analysis

Figure 5 shows the critical heat flux density when the aerosol is sprayed on the upper surface of the red copper specimen under different lubrication conditions. The critical heat flux density is the highest under CAEMQL, and this value is increased by 55.25%, 37.10%, and 22.84% compared to that obtained under MQL, EMQL, and CAMQL, respectively. According to the theory of enhanced heat transfer, with an increasing average heat transfer temperature difference, heat transfer coefficient, and heat transfer surface area, the heat transfer capacity can be improved [53]. The average heat transfer temperature difference of the copper specimen under CAMQL is enhanced, and when the cold air and low-temperature

**Fig. 9** Signal diagram of cutting temperature under different lubrication conditions: **a** MQL, **b** EMQL, **c** CAMQL, and **d** CAEMQL (cutting speed: 120 m/min; axial depth of cut: 1 mm; radial depth of cut: 5 mm; feed rate: 0.1 mm/tooth)



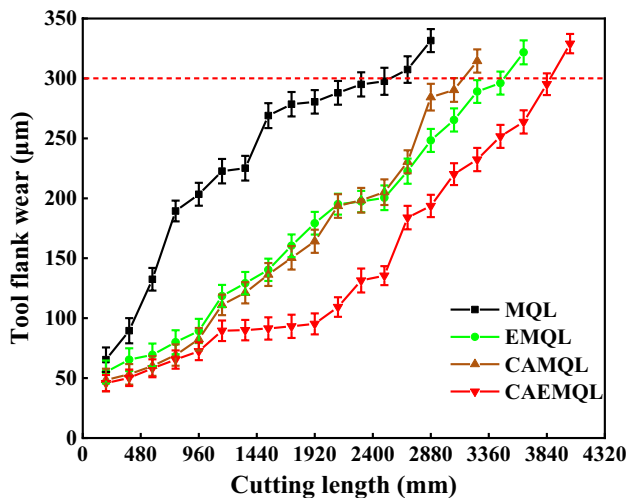


**Fig. 10** Flank wear with cutting length under different lubrication conditions (cutting speed: 120 m/min; axial depth of cut: 1 mm; radial depth of cut: 5 mm; feed rate: 0.1 mm/tooth)

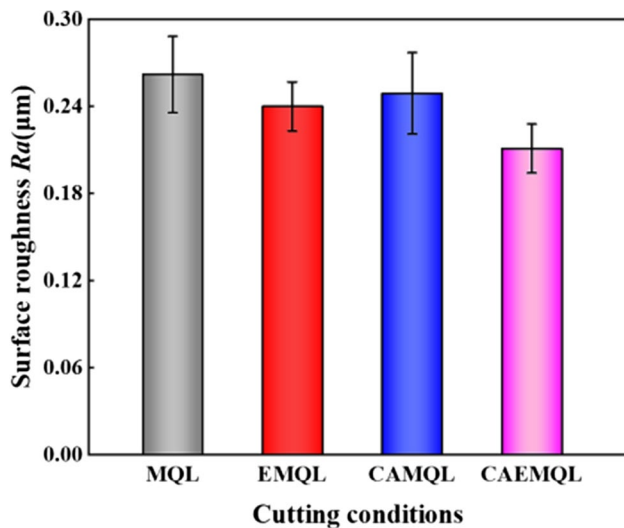


**Fig. 11** Workpiece surface roughness under different lubrication conditions (cutting speed: 120 m/min; axial depth of cut: 1 mm; radial depth of cut: 5 mm; feed rate: 0.1 mm/tooth)

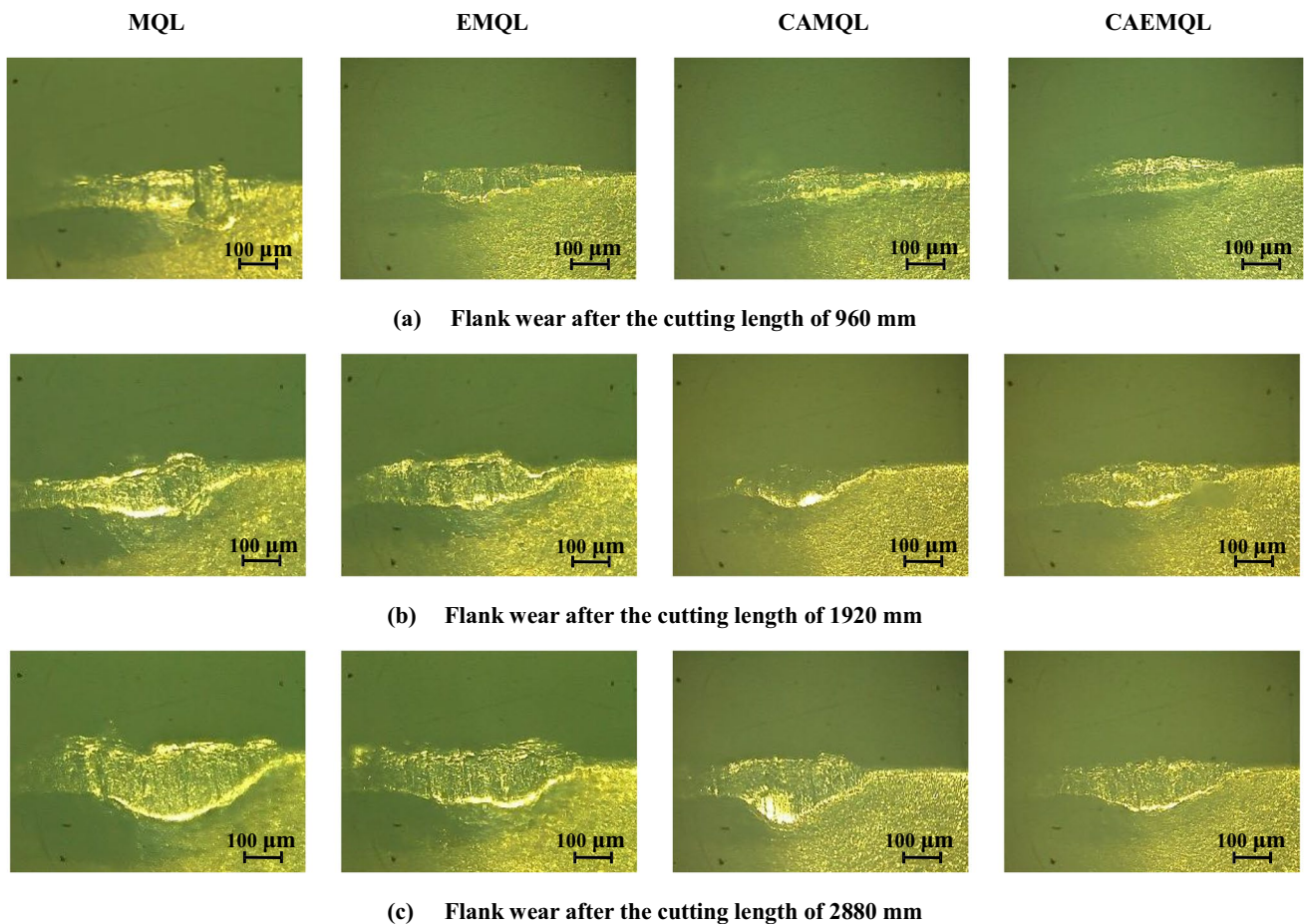
droplets touch the high-temperature surface, they quickly reduce the surface temperature and the possibility of film boiling [54], leading to better heat exchange efficiency. In addition, the convection heat transfer by cold air, heat conduction by oil mist sprayed on the copper specimen, and their boiling and evaporation also help heat dissipation. According to Huang et al. [48], charging can effectively reduce the particle size and contact angle of the droplets and promote the evaporation of the droplets, which allows a higher critical heat flux density to be obtained. Consequently, the transient heat transfer capacity of CAEMQL is stronger.

Figure 6 shows the steady-state heat transfer performance with the heating temperature under different lubrication conditions. CAEMQL results in the best steady-state heat transfer capability. As shown in Fig. 8a, b, when the heat exchange surface temperature is 170 °C, the surface heat flux density under CAEMQL is increased by 40.14%, 31.85%, and 20.72% and the steady-state heat transfer coefficient is increased by 35.57%, 20.21%, and 12.09% compared to those under MQL, EMQL, and CAMQL, respectively. According to the investigation by Xu et al. [11], EMQL has improved performance in terms of droplet deposition, uniformity, and wetting, which allows the droplets to enter and cover the heating sheet surface more easily, increases the area of heat exchange, and promotes evaporation. Moreover, the heat transfer coefficient under CAMQL is higher than that under MQL and EMQL. This may be attributed to the boiling and evaporation of lubricant oil droplets due to them absorbing the generated heat. In addition, the cold air sprays on the heat transfer surface and dissipates a large amount of heat by forced convection [13]. CAEMQL, which exerts a synergistic effect by combining CAMQL and EMQL, increases the temperature difference between the cold air and the heating sheet and promotes the evaporation of lubricant oil droplets, resulting in a higher heat exchange capacity. Consequently, the steady-state heat transfer performance of CAEMQL is better.

### 3.2 Milling performance under CAEMQL machining

Figure 7 shows the cutting force signals under different lubrication conditions. The average cutting force is shown in Fig. 8. It can be seen from Fig. 7a that the highest cutting force is obtained under MQL. This may be attributed to the lower heat transfer capacity, resulting in a higher coefficient of friction at the chip-tool interfaces. The cutting forces  $F_r$  under EMQL and CAMQL are lower than those under MQL machining, as shown in Fig. 7b, c, which may be attributed to the charged cutting fluid and cold air. According to an investigation by Lv et al. [50], when the cutting fluids are charged, the charged droplets have good permeability at the tool-chip and tool-workpiece interfaces, which is beneficial for forming a stable lubricating film, increasing the heat transfer area and the heat transfer capacity, and reducing the generation of friction heat, resulting in a reduction in cutting force. Although the low-temperature cooling effect improves the hardness of the workpiece material in the cold air environment to a certain extent, it also reduces the plasticity and toughness of the workpiece and decreases the adhesion of the workpiece material to the tool surface. Moreover, cold air can improve the convective heat transfer of aerosols and inhibit the temperature rise of the cutting area, which are beneficial for maintaining the tool's strength and leading to less





**Fig. 12** Optical micrograph of the tool flank wear after different cutting lengths under different lubrication conditions (cutting speed: 120 m/min; axial depth of cut: 1 mm; radial depth of cut: 5 mm; feed rate: 0.1 mm/tooth)

adhesive wear. Consequently, CAEMQL can further relieve the friction and adhesion at the tool-workpiece interfaces, resulting in a lower cutting force.

The change in cutting temperature under different lubrication conditions is shown in Fig. 9. The cutting temperature under CAEMQL is the lowest, and this value is reduced by 50.33%, 44.29%, and 13.23% compared to that under MQL, EMQL, and CAMQL, respectively. According to the heat transfer test, CAEMQL has a higher heat flux and heat transfer coefficient, resulting in a better heat transfer performance. At the same time, more lubricants penetrate into the machining area to participate in the cutting process, owing to the smaller particle size and contact angle of charged droplets, which can improve the friction in cutting interfaces and reduce the generation of friction heat, which is in agreement with the findings of Lin et al. [47]. Moreover, the cold air continuously cools at the tool-workpiece interfaces, which can improve the convective heat transfer ability of the aerosol and inhibit the temperature rise in the cutting area.

Figure 10 shows the progression of flank wear with the cutting length under different lubrication conditions. The

flank wear under MQL increases drastically with increasing cutting length. This may be attributed to the high machining area temperature and the increasing friction force at the tool-workpiece interface. As shown in Fig. 10, the growth of the tool flank wear under EMQL and CAMQL machining is lower than that under MQL machining. The cause of the reduction in flank wear may reasonably be attributed to the lower cutting force and cutting temperature, which are conducive to reducing tool wear and adhesive wear. However, when the cutting length exceeds 1920 mm, the tool flank wear under EMQL is lower than that under CAMQL, which shows that EMQL machining has a stronger lubrication characteristic for relieving the tool wear after the tool enters the stage of rapid wear.

It can be seen from Fig. 10 that CAEMQL provides the longest tool life, and its effective cutting length is 3744 mm, which is 33.33%, 7.69%, and 17.95% increased compared to that of MQL (2496 mm), EMQL (3456 mm), and CAMQL (3072 mm), respectively. This is attributed to the improved penetration, wetting, and deposition capabilities of the charged droplets, which facilitate a more efficient entry of

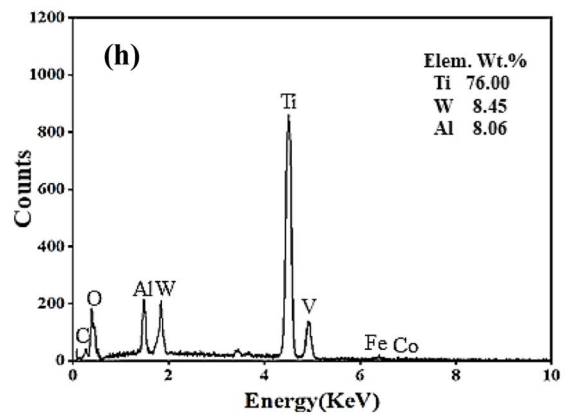
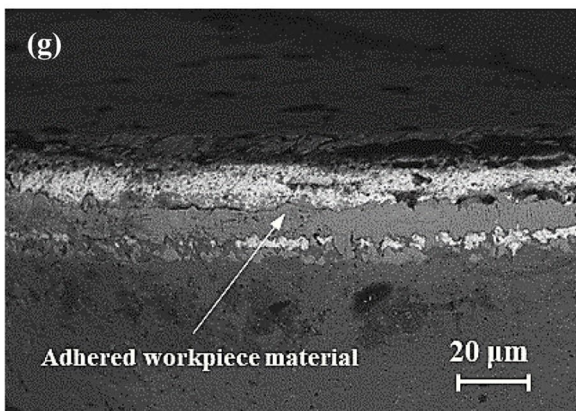
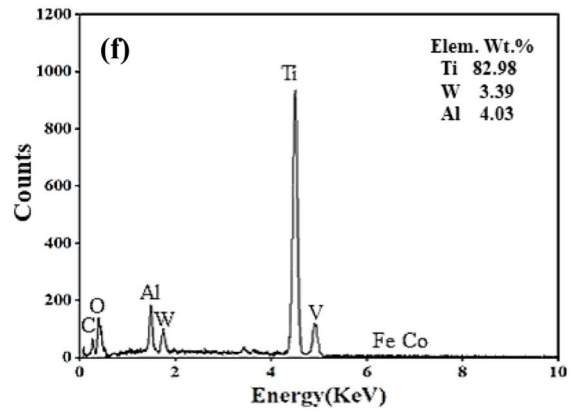
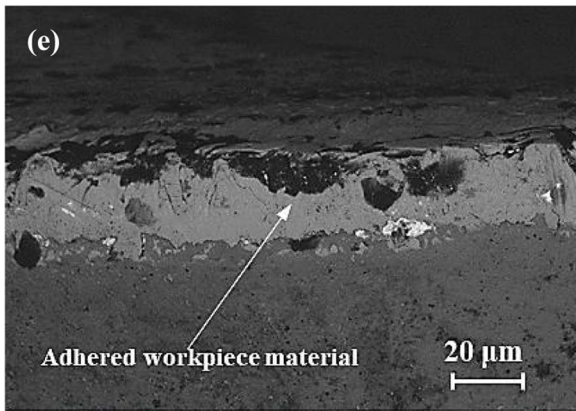
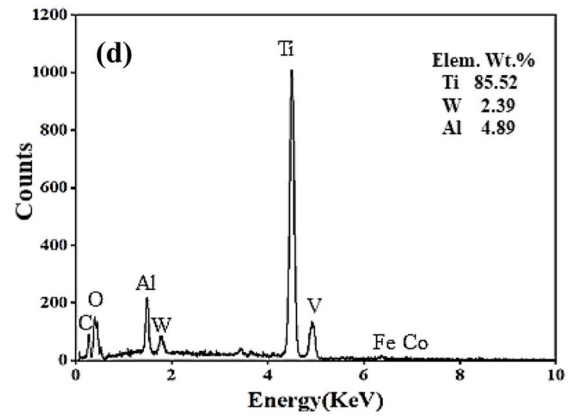
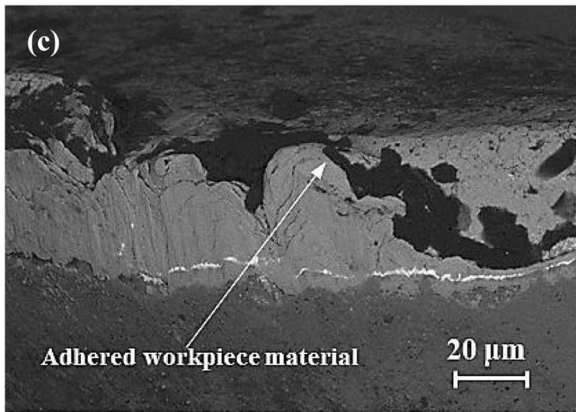
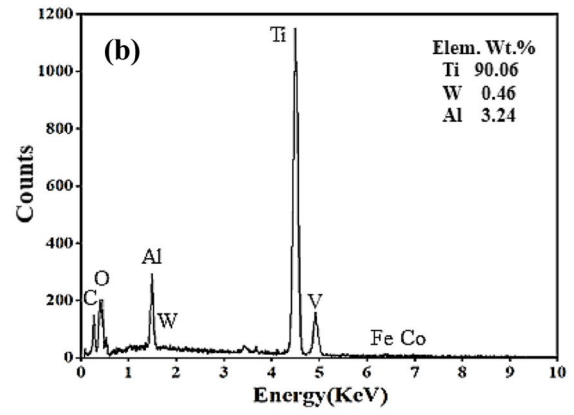
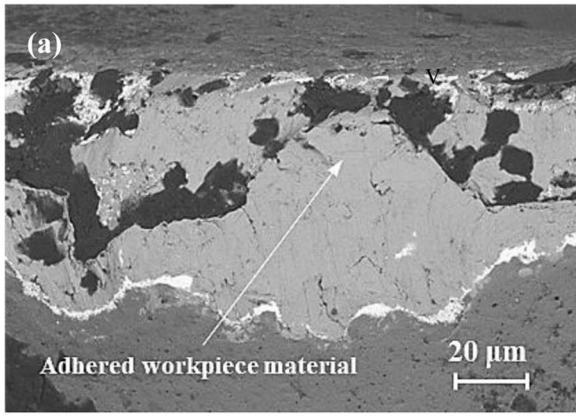


**Fig. 13** SEM micrographs and EDS images of tool flank wear under different lubrication conditions: **a, b** MQL, **c, d** EMQL, **e, f** CAMQL, and **g, h** CAEMQL (cutting length: 960 mm; cutting speed: 120 m/min; axial depth of cut: 1 mm; radial depth of cut: 5 mm; feed rate: 0.1 mm/tooth)

the lubricant into the machining area to promote the formation of the lubrication film, resulting in a reduction in the friction at the tool-workpiece interfaces. Moreover, the cold air helps to decrease the heat generation and adhesion of the tool's flank face. Consequently, CAEMQL can maintain strength and enhance the wear resistance of the cutting tool, resulting in a significant improvement in tool wear.

Figure 11 shows the workpiece surface roughness under different lubrication conditions. The average surface roughness under CAEMQL is the lowest, and this value is reduced by 25.15%, 17.28%, and 13.75% compared to that under MQL, EMQL, and CAMQL, respectively. This is because the better lubrication and cooling effect under CAEMQL reduce the scratches at the tool-workpiece interfaces and allow the chips to slide more smoothly over the tool surface, leading to less adhesion. However, the higher milling temperature under MQL leads to a strong thermal softening effect on the workpiece, which aggravates the adhesive wear of the tool. At the same time, the higher milling force deepens the scratches on the surface of the workpiece, which adversely affects the surface quality of the workpiece. As also shown in Fig. 11, the surface roughness under EMQL machining is lower than that under CAMQL machining. The cause of the reduction in surface roughness may reasonably be attributed to the better permeability of the charged droplets, which results in the reduction of tool wear and the alleviation of scratches at the tool-workpiece interfaces.

### 3.3 Tool failure modes

The optical micrographs of the tool flank wear with increasing cutting length under different lubrication conditions are shown in Fig. 12. When the milling length is 960 mm, different degrees of silver-colored adhesions are observed on the tool edge under various lubrication conditions, indicating that the tool wear mechanism is mainly adhesive wear. When the milling length reaches 1920 mm, the cutting edge under MQL and EMQL is passivated, and the tool flank wear begins to increase. Moreover, the flank wear under CAMQL is less than that under MQL and EMQL, which indicates that the cold air effectively reduces the milling temperature, obviously maintains the strength of the tool, and reduces adhesive wear. Compared to that under MQL, EMQL, and CAMQL, the tool flank wear under CAEMQL is the smallest, presenting a better tool wear inhibition ability. This is because the charged droplets can effectively enter the

tool-chip interfaces to participate in lubrication, and the cold air can be beneficial for maintaining tool strength, which corresponds to the tool life shown in Fig. 10.

Figure 13 shows the SEM and EDS analyses of the tool flank wear under different lubrication modes after a 960-mm cutting length. Different degrees of adhesions and furrows are observed on the tool flank faces under various lubrication conditions, indicating adhesive wear and abrasive wear. It can be seen in Fig. 13a, which shows the adhered workpiece materials on the flank surface of the worn tool under MQL. The corresponding EDS analysis shown in Fig. 13b detects high concentrations of titanium (Ti), indicating serious adhesive wear. Compared to that of MQL, EMQL, and CAMQL, the adhesive layer of CAEMQL is less, as shown in Fig. 13g. The corresponding EDS analysis shown in Fig. 13h detects higher concentrations of wolframium (W), which is the principal chemical element of the tool coating, and lower concentrations of Ti. The higher the concentrations of W are, the greater the integrity of the tool flank. This is because the charged droplets can enhance the wettability and permeability and effectively alleviate the adhesion wear. Moreover, cold air can reduce the cutting temperature, which is beneficial for maintaining the strength and hardness of the tool and reducing tool wear.

### 3.4 Chip morphology analysis

Chip morphology provides important clues about cutting mechanics and is closely related to surface roughness, cutting temperature, and tool flank wear [55, 56]. As shown in Fig. 14, the chip consists of a free surface, back surface (in contact with the tool rake face), top surface, and bottom surface. The formation of the chip is a common result of cutting load, material fracture, deformation, and friction properties of the contact interface in the process of milling cutting. This paper mainly analyzes the free surface and back surface morphology of titanium alloy Ti-6Al-4 V chips under different lubrication conditions.

When analyzing the free surface of a chip, the chip deformation degree is generally characterized by the degree of chip segmentation ( $G_s$ ) [57]. The definition formula is as follows:

$$G_s = (H - h)/H \quad (3)$$

Here,  $H$  is the peak chip height and  $h$  is the chip valley height. The specific measurement parameters are shown in Fig. 15.

Figure 16 shows the cross-section photographs of titanium alloy Ti-6Al-4 V chips under different lubrication conditions, which present a serrated shape. Figure 17 shows the average  $G_s$  under different lubrication conditions, which

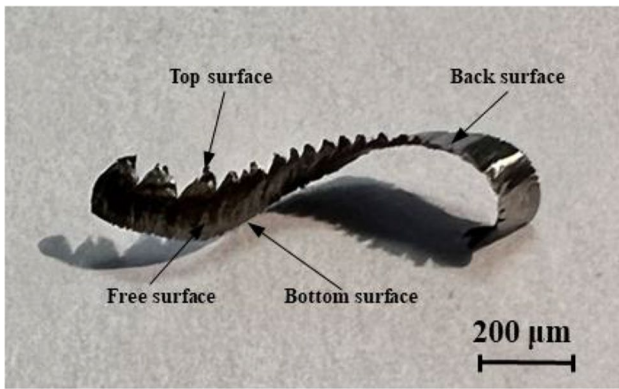


**Fig. 14** Physical diagram of the titanium alloy Ti-6Al-4 V chip

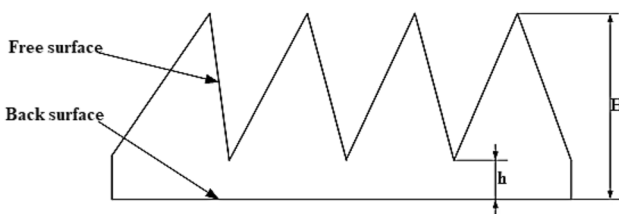
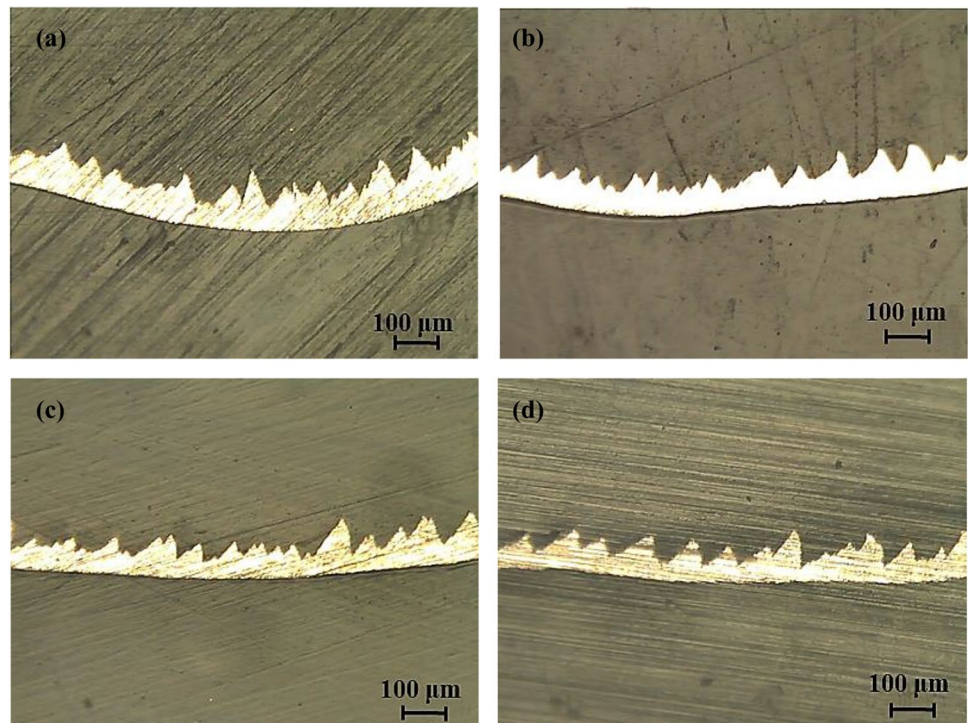


**Fig. 15** Schematic diagram of the serrated chip

are calculated by selecting the five highest degrees of chip segmentation. It can be seen that the highest average  $G_s$  are obtained under CAEMQL, and these values are 32.57%, 22.37%, and 5.33% higher than those obtained under MQL,

**Fig. 16** Metallographic serrated chips sample under different conditions: **a** MQL, **b** EMQL, **c** CAMQL, and **d** CAEMQL (cutting speed: 120 m/min; axial depth of cut: 1 mm; radial depth of cut: 5 mm; feed rate: 0.1 mm/tooth)



EMQL, and CAMQL, respectively. The size of the degree of chip segmentation depends on the size of the material failure strain [58].

As also shown in Fig. 17, the  $G_s$  under MQL are the smallest, which may be due to the higher milling temperature and material plasticity causing a larger failure strain, resulting in a lower  $G_s$ . The better lubrication performance of the charged droplets under EMQL can further enhance the  $G_s$ , which may be attributed to the decrease in milling forces and the reduction in milling temperature and failure strain to a certain extent. Moreover, the milling temperature under CAMQL is lower than that under EMQL and MQL, which further reduces the failure strain, resulting in a higher  $G_s$ . Consequently, the average  $G_s$  under CAEMQL are the highest.

In cutting, the back surface of the chip is in contact with the rake face of the tool and undergoes plastic deformation as it slides across the rake face due to high contact stress, shear stress, and friction force [59, 60]. Figure 18 shows the back surface morphology of chips under different lubrication conditions. It can be seen that there are obvious scratches on the back surface of the chips. According to Tang [56], the chip back surface is the contact surface between the chip and the tool rake surface, and its scratches are the cumulative result of friction forces, contact pressure, and high temperature. As shown in Fig. 18a, a larger cutting force leads to deeper scratches and concave deformation on the back surface under MQL, which reflect poor cutting performance. As seen in Fig. 18b, the scratches under EMQL are

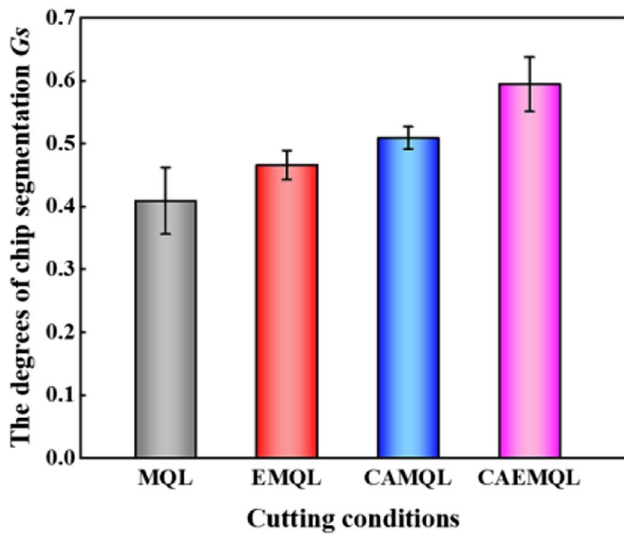
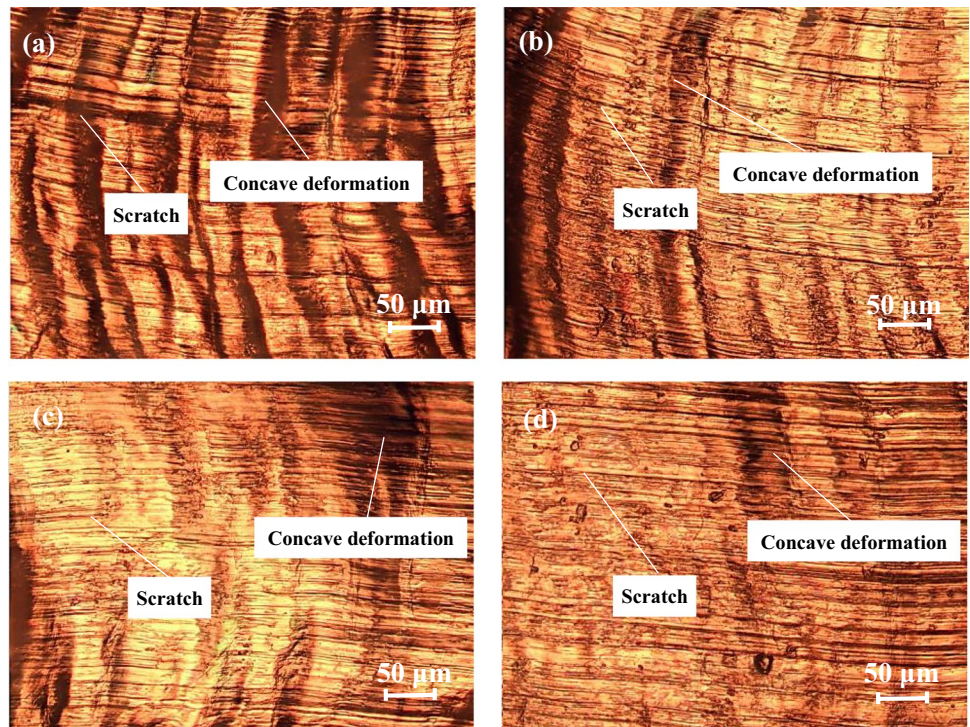


**Fig. 17** Degrees of chip segmentation under different lubrication conditions

alleviated due to the smaller friction between the tool and chip and the strong wetting and lubricating ability of the charged droplets.

Figure 18c shows that there are shallower scratches and smaller concave deformations under CAMQL. This is because the cold air reduces the milling temperature in the cutting area, increases the chip hardness, and decreases the tool adhesion. Furthermore, as seen in Fig. 18d, with the synergistic effect of charged droplets and cold air,

**Fig. 18** Back surface morphology of chips under different lubrication conditions: **a** MQL, **b** EMQL, **c** CAMQL, and **d** CAEMQL (cutting speed: 120 m/min; axial depth of cut: 1 mm; radial depth of cut: 5 mm; feed rate: 0.1 mm/tooth)



the scratches and concave deformation under CAEMQL are the smallest, which indicates that this method can improve friction in the cutting area, enhancing milling performance.

### 4 Conclusions

To decrease the cutting temperature in the cutting area and prolong the tool life, a lubrication/cooling method called CAEMQL was proposed. The heat transfer characteristics of CAEMQL were comparatively analyzed. The comparative performance analysis of CAEMQL, MQL, EMQL, and CAMQL machining in terms of milling titanium alloy and chip morphology was systematically investigated through experiments. According to the experimental results, the corresponding conclusions are listed as follows:

(1) The critical heat flux, heat flux density, and heat transfer coefficient under CAEMQL were higher than those under MQL, EMQL, and CAMQL, respectively. The cold air increased the temperature difference between the specimens and improved the convective heat exchange ability. The charged droplets increased the contact area of the specimen and the evaporation heat exchange efficiency.

(2) In the milling process of the titanium alloy Ti–6Al–4 V, a lower milling force, smaller milling temperature, and better surface quality under CAEMQL were obtained. At the same time, the tool life under CAEMQL was longer than that under MQL, EMQL, and CAMQL.

(3) The optical micrograph of the tool flank showed that the adhesion layer and wear of the tool flank under CAEMQL were the least compared to those under MQL, EMQL, and CAMQL. The SEM and EDS analyses showed that the tool flank mainly underwent adhesive wear and abrasive wear. The concentrations of Ti under MQL were the highest, while the concentrations of Ti were the lowest and the concentrations of W were the highest under CAEMQL.

(4) The low-temperature cooling effect reduced the failure stain, and the lubrication enhancement effect of the charged droplets decreased the friction at the tool-chip interfaces under CAEMQL in the milling process, which led to an increase in the degrees of chip segmentation  $G_s$ . Moreover, the scratches on the back surface of the chips were shallower and smoother.

**Author contribution** All the authors have contributed to the creation of this manuscript for its important intellectual content and approved the final manuscript. Xuefeng Xu: methodology, data curation, experimentation, validation, formal analysis, and writing—review, and editing. Fucai Liu: supervision, writing—original draft, and writing—review and providing method. Yu Xia and Tao Lv: supervision and guidance. Ruochong Zhang and Xiaodong Hu: experimentation and analysis of the data.

**Funding** The work described in this paper was supported by the China National Key R&D Program (Grant No. 52275468).

**Data availability** All data generated or analyzed during this study are included in this published article.

**Code availability** Not applicable.

## Declarations

**Ethics approval** The authors confirm the work's novelty and state that it has not been submitted to any other journal.

**Consent to participate** The authors give consent to participate.

**Consent for publication** The authors give their consent for their work to be published.

**Conflict of interest** The authors declare no conflict of interest.

## References

- Dong G, Gao S, Wang L (2022) Three dimensional shape model of TiBw mesh reinforced titanium matrix composites in rotary ultrasonic grinding. *J Manuf Process* 75:682–692. <https://doi.org/10.1016/j.jmapro.2022.01.039-tihuan>
- Fernandez DS, Wynne BP, Crawforth P, Jackson M (2021) Titanium alloy microstructure fingerprint plots from in-process machining. *Mat Sci Eng A-Struct* 811 <https://doi.org/10.1016/j.msea.2021.141074>
- Babaremu KO, Jen TC, Oladijo PO, Akinlabi ET (2022) Mechanical, corrosion resistance properties and various applications of titanium and its alloys: a review. *Revue Des Composites Et Des Materiaux Avances-Journal of Composite and Advanced Materials* 32:11–16. <https://doi.org/10.18280/rcma.320102>
- Pramanik A, Littlefair G (2015) Machining of titanium alloy (Ti-6Al-4V)-theory to application. *Mach Sci Technol* 19:1–49. <https://doi.org/10.1080/10910344.2014.991031>
- Jung HJ, Hayasaka T, Shamoto E, Xu LJ (2020) Suppression of forced vibration due to chip segmentation in ultrasonic elliptical vibration cutting of titanium alloy Ti-6Al-4V. *Precis Eng* 64:98–107. <https://doi.org/10.1016/j.precisioneng.2020.03.017>
- Jia D, Zhang Y, Li C, Yang M, Gao T, Said Z, Sharma S (2022) Lubrication-enhanced mechanisms of titanium alloy grinding using lecithin biolubricant. *Tribol Int* 169 <https://doi.org/10.1016/j.triboint.2022.107461>
- Damm O, Bezuidenhout M, Uheida E, Dicks L, Hadasha W, Hagedorn-Hansen D (2021) Yeast-based metalworking fluid for milling of titanium alloy - an example of bio-integration. *CIRP J Manuf Sci Tec* 34:47–60. <https://doi.org/10.1016/j.cirpj.2021.01.004>
- Wu X, Li C, Zhou Z, Nie X, Chen Y, Zhang Y, Cao H, Liu B, Zhang N, Said Z, Debnath S, Jamil M, Ali HM, Sharma S (2021) Circulating purification of cutting fluid: an overview. *Int J Adv Manuf Technol* 117:2565–2600. <https://doi.org/10.1007/s00170-021-07854-1>
- Lian Y, Long Y, Zhao G, Mu C, Li X, Deng J, Xie C (2020) Performance of CrCN-WS2 hard/soft composite coated tools in dry cutting of titanium alloys. *J Manuf Process* 54:201–209. <https://doi.org/10.1016/j.jmapro.2020.03.014>
- Zhang S, Li J, Wang Y (2012) Tool life and cutting forces in end milling Inconel 718 under dry and minimum quantity cooling lubrication cutting conditions. *J Clean Prod* 32:81–87. <https://doi.org/10.1016/j.jclepro.2012.03.014>
- Xu X, Huang S, Wang M, Yao W (2017) A study on process parameters in end milling of AISI-304 stainless steel under electrostatic minimum quantity lubrication conditions. *Int J Adv Manuf Technol* 90:979–998. <https://doi.org/10.1007/s00170-016-9417-3>
- Wu G, Li G, Pan W, Raja I, Wang X, Ding S (2022) Experimental investigation of eco-friendly cryogenic minimum quantity lubrication (CMQL) strategy in machining of Ti-6Al-4V thin-wall part. *J Clean Prod* 357 <https://doi.org/10.1016/j.jclepro.2022.131993>
- Saberi A, Rahimi A, Parsa H, Ashrafiyou M, Rabiei F (2016) Improvement of surface grinding process performance of CK45 soft steel by minimum quantity lubrication (MQL) technique using compressed cold air jet from vortex tube. *J Clean Prod* 131:728–738. <https://doi.org/10.1016/j.jclepro.2016.04.104>
- Yildiz Y, Nalbant M (2008) A review of cryogenic cooling in machining processes. *Int J Mach Tool Manuf* 48:947–964. <https://doi.org/10.1016/j.ijmactools.2008.01.008>
- Okada M, Hosokawa A, Asakawa N, Ueda T (2014) End milling of stainless steel and titanium alloy in an oil mist environment. *Int J Adv Manuf Technol* 74:1255–1266. <https://doi.org/10.1007/s00170-014-6060-8>
- Wang X, Li C, Zhang Y, et al (2022) Tribology of enhanced turning using biolubricants: a comparative assessment. *Tribol Int* 174 <https://doi.org/10.1016/j.triboint.2022.107766>
- Osman K, Ünver H, Seker U (2019) Application of minimum quantity lubrication techniques in machining process of titanium alloy for sustainability: a review. *Int J Adv Manuf Technol* 100:2311–2332. <https://doi.org/10.1007/s00170-018-2813-0>
- Sartori S, Ghiotti A, Bruschi S (2018) Solid lubricant-assisted minimum quantity lubrication and cooling strategies to improve Ti6Al4V machinability in finishing turning. *Tribol Int* 118:287–294. <https://doi.org/10.1016/j.triboint.2017.10.010>

19. Mia M, Gupta M, Lozano J, Carou D, Pimenov D, Królczyk G et al (2019) Multi-objective optimization and life cycle assessment of eco-friendly cryogenic N<sub>2</sub> assisted turning of Ti-6Al-4V. *J Clean Prod* 210:121–133. <https://doi.org/10.1016/j.jclepro.2018.10.334>
20. Maruda R, Krolczyk G, Nieslony P, Wojciechowski S, Michalski M, Legutko S (2016) The influence of the cooling conditions on the cutting tool wear and the chip formation mechanism. *J Manuf Process* 24:107–115. <https://doi.org/10.1016/j.jmapro.2016.08.006>
21. Maruda R, Krolczyk G, Feldshtein E, Nieslony P, Tyliszczak B, Pusavec F (2017) Tool wear characterizations in finish turning of AISI 1045 carbon steel for MQCL conditions. *Wear* 372–373:54–67. <https://doi.org/10.1016/j.wear.2016.12.006>
22. Maruda R, Krolczyk G, Michalski M, Nieslony P, Wojciechowski S (2017) Structural and microhardness changes after turning of the AISI 1045 steel for minimum quantity cooling lubrication. *J Mater Eng Perform* 26:431–438. <https://doi.org/10.1007/s11665-016-2450-4>
23. Pal A, Chatha S, Sidhu H (2021) Performance evaluation of the minimum quantity lubrication with Al<sub>2</sub>O<sub>3</sub>-mixed vegetable-oil-based cutting fluid in drilling of AISI 321 stainless steel. *J Manuf Process* 66:238–249. <https://doi.org/10.1016/j.jmapro.2021.04.024>
24. Rodriguez R, Lopes J, Hildebrandt R, Perez R et al (2019) Evaluation of grinding process using simultaneously MQL technique and cleaning jet on grinding wheel surface. *J Mater process tech* 271:357–367. <https://doi.org/10.1016/j.jmatprotec.2019.03.019>
25. Şirin S, Sarıkaya M, Yıldırım C, Kivak T (2021) Machinability performance of nickel alloy X-750 with SiAlON ceramic cutting tool under dry, MQL and hBN mixed nanofluid-MQL. *Tribol Int* 153:106673. <https://doi.org/10.1016/j.triboint.2020.106673>
26. Sarıkaya M, Gupta M, Tomaz I, Danish M, Mia M, Rubaiee S et al (2021) Cooling techniques to improve the machinability and sustainability of light-weight alloys: a state-of-the-art review. *J Manuf Process* 62:179–201. <https://doi.org/10.1016/j.jmapro.2020.12.013>
27. Dhar N, Ahmed M, Islam S (2007) An experimental investigation on effect of minimum quantity lubrication in machining AISI 1040 steel. *Int J Mach Tool Manuf* 47:748–753. <https://doi.org/10.1016/j.ijmachtools.2006.09.017>
28. Tasdelen B, Thordenberg H, Olofsson D (2008) An experimental investigation on contact length during minimum quantity lubrication (MQL) machining. *J Mater Process Tech* 203:221–231. <https://doi.org/10.1016/j.jmatprotec.2007.10.027>
29. Krishnan P, Raj S (2022) Analysis of high speed drilling AISI 304 under MQL condition through a novel tool wear measurement method and surface integrity studies. *Tribol Int* 176 <https://doi.org/10.1016/j.triboint.2022.107871>
30. Sun H, Zou B, Chen P, Huang C, Guo G, Liu J, Li L, Shi Z (2022) Effect of MQL condition on cutting performance of high-speed machining of GH4099 with ceramic end mills. *Tribol Int* 167 <https://doi.org/10.1016/j.triboint.2021.107401>
31. Shen B (2008) Minimum quantity lubrication grinding using nanofluids. Doctoral dissertation, University of Michigan <https://hdl.handle.net/2027.42/60683>
32. Yuan S, Yan L, Liu W, Liu Q (2011) Effects of cooling air temperature on cryogenic machining of Ti-6Al-4V alloy. *J Mater Process Tech* 211:356–362. <https://doi.org/10.1016/j.jmatprotec.2010.10.009>
33. Silva L, Correa E, Brandao J, Avila R (2020) Environmentally friendly manufacturing: behavior analysis of minimum quantity of lubricant - MQL in grinding process. *J Clean Prod* 256 10.1016/j.jclepro.2013.01.033
34. Jamil M, He N, Huang X, Zhao W, Khan A, Asifqbal (2022) Thermophysical, tribological, and machinability characteristics of newly developed sustainable hybrid lubri-coolants for milling Ti-6Al-4V. *J Manuf Process* 73:572–594. <https://doi.org/10.1016/j.jmapro.2021.10.051>
35. Cetindag H, Cicek A, Ucak N (2020) The effects of CryoMQL conditions on tool wear and surface integrity in hard turning of AISI 52100 bearing steel. *J Manuf Process* 56:463–473. <https://doi.org/10.1016/j.jmapro.2020.05.015>
36. Gross D, Hanenkamp N (2021) Energy efficiency assessment of cryogenic minimum quantity lubrication cooling for milling operations. *Procedia CIRP* 98:523–528. <https://doi.org/10.1016/j.procir.2021.01.145>
37. Sanchez JA, Pombo I, Alberdi R, Izquierdo B, Ortega N, Plaza S, Martinez-Toledano J (2010) Machining evaluation of a hybrid MQL-CO<sub>2</sub> grinding technology. *J Clean Prod* 18:1840–1849. <https://doi.org/10.1016/j.jclepro.2010.07.002>
38. Hong S, Ding Y (2001) Cooling approaches and cutting temperatures in cryogenic machining of Ti-6Al-4V. *Int J Mach Tool Manuf* 41:1417–1437. [https://doi.org/10.1016/S0890-6955\(01\)00026-8](https://doi.org/10.1016/S0890-6955(01)00026-8)
39. Jebaraj M, Kumar MP, Anburaj R (2020) Effect of LN<sub>2</sub> and CO<sub>2</sub> coolants in milling of 55NiCrMoV7 steel. *J Manuf Process* 53:318–327. <https://doi.org/10.1016/j.jmapro.2020.02.040>
40. Ravi S, Gurusamy P (2019) Experimental studies on the effect of LN<sub>2</sub> cooling on the machining of tool steel. *Mater Today: Proc* 33:3292–3296. <https://doi.org/10.1016/j.matpr.2020.04.734>
41. Yang Y, Guo S, Si L, Liu T, Dai Y, Yan C (2021) Investigation of a new water-based cutting fluid for machining of titanium alloys. *J Manuf Process* 71:398–406. <https://doi.org/10.1016/j.jmapro.2021.09.046>
42. Shokrani A, Al-Samarrai I, Newman S (2019) Hybrid cryogenic MQL for improving tool life in machining of Ti-6Al-4V titanium alloy. *J Manuf Process* 43:229–243. <https://doi.org/10.1016/j.jmapro.2019.05.006>
43. Lin H, Wang C, Yuan Y, Chen Z, Wang Q, Xiong W (2015) Tool wear in Ti-6Al-4V alloy turning under oils on water cooling comparing with cryogenic air mixed with minimal quantity lubrication. *Int J Adv Manuf Technol* 81:87–101. <https://doi.org/10.1007/s00170-015-7062-x>
44. Zhang G, Wei H (2010) Selection of optimal process parameters for gear hobbing under cold air minimum quantity lubrication cutting environment. Proceedings of the 36th International MATA-DOR Conference 231–234 [https://doi.org/10.1007/978-1-84996-432-6\\_53](https://doi.org/10.1007/978-1-84996-432-6_53)
45. Mitrofanov A, Parsheva K, Nosenko V (2021) Simulation of an artificial neural network for predicting temperature and cutting force during grinding using CAMQL. *Mater Today: Proc* 38:1508–1511. <https://doi.org/10.1016/j.matpr.2020.08.139>
46. Krutikova A, Mitrofanov A, Parsheva K (2019) Application of the technology of supplying a minimum amount of lubricant in a cooled air stream when grinding a heat-resistant alloy. *Tekhnologiya Metallov* 8:9–15
47. Lin J, Lv T, Huang S, Hu X, Xu X (2018) Experimental investigation on grinding performance based on EMQL technology. *Chin J Mech Eng* 29:2783–2791. <https://doi.org/10.3969/j.issn.1004-132X.2018.23.003>
48. Huang S, Wang Z, Yao W, Xu X (2015) Tribological evaluation of contact-charged electrostatic spray lubrication as a new near-dry machining technique. *Tribol Int* 91:74–84. <https://doi.org/10.1016/j.triboint.2015.06.029>
49. Huang S, Lv T, Wang M, Xu X (2018) Effects of machining and oil mist parameters on electrostatic minimum quantity lubrication-EMQL turning process. *Int J of Precis Eng and Manuf-Green Tech* 5:317–326. <https://doi.org/10.1007/s40684-018-0034-5>
50. Lv T, Xu X, Yu A, Hu X (2021) Oil mist concentration and machining characteristics of SiO<sub>2</sub> water-based nano-lubricants

- in electrostatic minimum quantity lubrication-EMQL milling. *J Mater Process Tech* 290 <https://doi.org/10.1016/j.jmatprotec.2020.116964>
51. Bartolomeis AD, Newman ST, Shokrani A (2021) High-speed milling Inconel 718 using electrostatic minimum quantity lubrication (EMQL). *Procedia CIRP* 101:354–357. <https://doi.org/10.1016/j.procir.2021.02.038>
52. Jia D, Li C, Zhang Y, Yang M, Cao H, Liu B, Zhou Z (2022) Grinding performance and surface morphology evaluation of titanium alloy using electric traction bio micro lubricant. *J Mech Eng* 58(198–211):1. <https://doi.org/10.3901/JME.2022.05.198>
53. Wendelstorf J, Spitzer K, Wendelstorf R (2008) Spray water cooling heat transfer at high temperatures and liquid mass fluxes. *Int J Heat Mass Tran* 51:4902–4910. <https://doi.org/10.1016/j.ijheatmasstransfer.2008.01.032>
54. Tan W (2001) Computer simulation of a spray cooling system with FC-72. Doctoral dissertation, Orlando: University of Central Florida
55. Yildirim C, Kivak T, Sarikaya M, Sirin S (2020) Evaluation of tool wear, surface roughness/topography and chip morphology when machining of Ni-based alloy 625 under MQL, cryogenic cooling and CryoMQL. *J Mater Res Technol* 9(2020):2079–2092. <https://doi.org/10.1016/j.jmrt.2019.12.069>
56. Asad M, Ijaz H, Khan M, Khan M, Mabrouki T, Rashid M (2022) Comparative analyses and investigations of chamfered and honed-edge tool geometries on tool wear, chip morphology, residual stresses and end-burr formation. *J Manuf Process* 80:196–209. <https://doi.org/10.1016/j.mapro.2022.06.004>
57. Zhao Y, Li J, Guo K, Sivalingam V, Sun J (2020) Study on chip formation characteristics in turning NiTi shape memory alloys. *J Manuf Process* 58:787–795. <https://doi.org/10.1016/j.jmapro.2020.08.072>
58. Wang B, Liu Z, Su G, Ai X (2015) Brittle removal mechanism of ductile materials with ultrahigh-speed machining. *J Manuf Sci E-T Asme* 137 <https://doi.org/10.1115/1.4030826>
59. Hariprasad B, Selvakumar S, Raj S (2022) Effect of cutting edge radius on end milling Ti–6Al–4V under minimum quantity cooling lubrication – chip morphology and surface integrity study. *Wear* 498–499 <https://doi.org/10.1016/j.wear.2022.204307>
60. Tang L, Li P, Qiu X, Niu Q (2018) Study on surface morphology and burr of titanium alloy TC4 turned with carbide coated insert. *Tool Eng* 52:52–55. <https://doi.org/10.3969/j.issn.1000-7008.2018.08.030>

**Publisher's note** Springer Nature remains neutral with regard to jurisdictional claims in published maps and institutional affiliations.

Springer Nature or its licensor (e.g. a society or other partner) holds exclusive rights to this article under a publishing agreement with the author(s) or other rightsholder(s); author self-archiving of the accepted manuscript version of this article is solely governed by the terms of such publishing agreement and applicable law.